Journal of the American Mosquito Control Association, 39(2):96–107, 2023

A HABITAT MODEL FOR DISEASE VECTOR *AEDES AEGYPTI* IN THE TAMPA BAY AREA, FLORIDA

JOHNNY A. UELMEN JR.,[1] CONNOR D. MAPES,[1] AGNE PRASAUSKAS,[2] CARL BOOHENE,[3] LEONARD BURNS,[4] JASON STUCK[5] AND RYAN M. CARNEY[1]

ABSTRACT. Within the contiguous USA, Florida is unique in having tropical and subtropical climates, a great abundance and diversity of mosquito vectors, and high rates of human travel. These factors contribute to the state being the national ground zero for exotic mosquito-borne diseases, as evidenced by local transmission of viruses spread by *Aedes aegypti*, including outbreaks of dengue in 2022 and Zika in 2016. Because of limited treatment options, integrated vector management is a key part of mitigating these arboviruses. Practical knowledge of when and where mosquito populations of interest exist is critical for surveillance and control efforts, and habitat predictions at various geographic scales typically rely on ecological niche modeling. However, most of these models, usually created in partnership with academic institutions, demand resources that otherwise may be too time-demanding or difficult for mosquito control programs to replicate and use effectively. Such resources may include intensive computational requirements, high spatiotemporal resolutions of data not regularly available, and/or expert knowledge of statistical analysis. Therefore, our study aims to partner with mosquito control agencies in generating operationally useful mosquito abundance models. Given the increasing threat of mosquito-borne disease transmission in Florida, our analytic approach targets recent *Ae. aegypti* abundance in the Tampa Bay area. We investigate explanatory variables that: 1) are publicly available, 2) require little to no preprocessing for use, and 3) are known factors associated with *Ae. aegypti* ecology. Out of our 4 final models, none required more than 5 out of the 36 predictors assessed (13.9%). Similar to previous literature, the strongest predictors were consistently 3- and 4-wk temperature and precipitation lags, followed closely by 1 of 2 environmental predictors: land use/land cover or normalized difference vegetation index. Surprisingly, 3 of our 4 final models included one or more socioeconomic or demographic predictors. In general, larger sample sizes of trap collections and/or citizen science observations should result in greater confidence in model predictions and validation. However, given disparities in trap collections across jurisdictions, individual county models rather than a multicounty conglomerate model would likely yield stronger model fits. Ultimately, we hope that the results of our assessment will enable more accurate and precise mosquito surveillance and control of *Ae. aegypti* in Florida and beyond.

KEY WORDS Geographic information system, mosquito control, precipitation, spatial modeling, temperature

INTRODUCTION

Dengue and Zika are dangerous arboviruses endemic to tropical and subtropical regions (Kraemer et al. 2015a, Patterson et al. 2016). Approximately half the world's population is currently at risk, and 390 million people are infected by dengue annually (WHO 2021). The rapid global rise in dengue occurrence may have immense public health implications for future transmission in Florida (Wilder-Smith et al. 2019), which is particularly vulnerable. The state's proximity to arbovirus-endemic areas, the hub for tourism, and the warm and humid climate provide the ideal environment for exotic mosquitoes and mosquito-borne pathogens to be introduced and transmitted (Beeman et al. 2021, Reeves et al. 2023). Indeed, in 2022, Florida was the only state with locally transmitted cases of dengue ($n = 47$; CDC 2022), and local outbreaks and isolated introductions of dengue virus occasionally occur in South Florida (Rey 2014). Locally acquired dengue infections have also been documented in the Tampa Bay area in 1905, 1907, 1934, 2011, and 2019 (Rey 2014, FDH 2021). In 2016, an outbreak of Zika virus occurred in Miami-Dade and Broward counties, resulting in at least 300 human cases (Likos et al. 2016).

The primary vector that spreads dengue, Zika, and yellow fever is *Aedes aegypti* (F.), a highly successful invasive species (Gardner et al. 2017) with a geographic range that is very likely to expand, largely fueled by human transportation and changing climate (Kamal et al. 2018). *Aedes aegypti* is highly anthropophilic and strongly associated with human environments (Takken and Verhulst 2013), and typically breeds in small and often artificial outdoor containers that gather rainwater in urban and suburban areas (Kraemer et al. 2015a). *Aedes aegypti* has been present in the Americas since the 15th century, with seasonal distributions documented as far north as New Jersey (Donnelly 1993), and crucially is present year-round throughout Florida (Kraemer et al. 2015b, 2019; CDC 2017).

[1] Department of Integrative Biology, University of South Florida, 4202 E Fowler Avenue, Tampa, FL 33620.
[2] Pasco County Mosquito Control District, 2308 Marathon Road, Odessa, FL 33556.
[3] Polk County Mosquito Control, 4177 Ben Durrance Road, Bartow, FL 33830.
[4] Hillsborough County Mosquito Management Services, 601 E Kennedy Boulevard, Tampa, FL 33602.
[5] Pinellas County Mosquito Control, 22211 US Highway 19 North, Clearwater, FL 33765.

Table 1. Average number of female *Aedes aegypti* collected each month between 2017 and 2019 by county and trap type. Statistical significance (Tukey–Kramer HSD) denoted by asterisk ($P < 0.05$). Note that overall averages are based on original weighted counts and not the averages, and do not include zero counts.

	County									
	Hillsborough		Pasco		Pinellas			Polk		
Month	BG-Sentinel*	CDC light trap[1]	CDC light trap	Suction trap	BG-Sentinel*	CDC light trap*	Wilton trap	BG-Sentinel	CDC light trap	Overall average by month
Jan		1.6	3.8		15.5	2.1			2.7	8.0
Feb		1.6	2.2		11.1	1		1.5	3	6.1
Mar*	1	1.5	1.9	1.3	9.7	1.5			1.5	7.7
Apr*	5	1.8	1.5	1.3	14.2	1.4		1	3.1	8.4
May	15.3	1.5	3.5	1.3	20.3	1.4		1.6	3.1	11.9
June*	114.2	3.5	10.0	2.1	70.5			28.5	3.7	28.7
July	36.5	3.6	5.5	2.3	44.5	6.4	8	58	7.7	21.1
Aug	85.9	3.0	11.4	1.5	31.4	3.2	7.5	6	6.4	23.1
Sep	15.3	2	1.3	1.4	14.5	1.2	2		4.4	8.8
Oct	5.2	2.1	1.8	1.3	15.0	1.9	5.3	4.1	5.7	10.0
Nov	10.7	1.4	1.8	1.2	11.5	1.8	22	1.7	2.1	7.1
Dec	1	1.2	1.8		5.8			1	4.6	4.5
Overall average per trap type	50.0	2.6	5.4	1.8	27.0	3.1	9.0	10.9	4.1	16.7
Overall average per county	25.5		2.3		12.3			5.6		

[1] CDC, Centers for Disease Control and Prevention.

Previous studies in Florida have shown that *Ae. aegypti* habitats are highly dependent on surrounding land cover and are typically found in residential areas (Leisnham et al. 2014). In tropical southern Taiwan, Huang et al. (2018) found that dengue transmission was associated with urban areas and parks, as well as decreasing areas of green space, particularly in conjunction with increasing built environments. *Aedes aegypti* is limited by seasonal environmental conditions and is more active during specific times of the year. Monaghan et al. (2019) constructed a US-based model based on meteorological data and found the greatest *Ae. aegypti* abundance in September and a generally high abundance from July to October in the southeastern USA. Given the climate of Florida, there may be an even longer period associated with high *Ae. aegypti* abundance.

As one of the fastest growing regions in the USA, the Tampa Bay area has experienced an influx of population, resulting in the expansion of built environments after thousands of acres of agricultural, forest, and scrub lands were cleared to make way for new homes and businesses (Hartz 2022). These disturbed environments create ideal breeding habitats for *Ae. aegypti* and increase the potential for arbovirus transmission in counties of the Tampa Bay area (here including Hillsborough, Pasco, Pinellas, and Polk). Fortunately, each of these counties maintains year-round mosquito control agencies with high-quality historic trap data. For all of the above reasons, the Tampa Bay area is an ideal region for modeling *Ae. aegypti* abundance.

With no specific treatments for either dengue or Zika, prevention measures such as frequent mosquito surveillance and targeted control are paramount for public health. Our study caters to mosquito control agencies by developing an *Ae. aegypti*–specific abundance model using data sources that are easily accessible, to produce results that have practical, operational utility. Ultimately, the techniques and suggestions proposed in this study aim to increase the efficiency of mosquito control efforts in targeting high-abundance locations in time and space, thereby reducing vector and virus exposure to humans.

MATERIALS AND METHODS

Datasets

All mapping and geographic information system applications were conducted in ArcMap (10.8; Environmental System Research Institute, Redlands, CA). Mosquito abundance and date of collections provided the spatiotemporal data for the dependent variables in the habitat models. Female *Ae. aegypti* abundance from January 1, 2017, to December 31, 2019, was provided by the mosquito control programs from each of the 4 counties within the Tampa Bay area: Hillsborough (2,600 km^2), Pasco (1,930 km^2), Pinellas (710 km^2), and Polk (4,660 km^2). Abundance data were acquired from 497 mosquito traps of 4 common types: BG-Sentinel ($n = 314$), Centers for Disease Control and Prevention (CDC) light ($n = 135$), suction ($n = 39$), and Wilton ($n = 9$); however, only CDC light traps were used in all counties (Table 1 and Fig. 1A). Furthermore, to account for differences in productivity, traps were

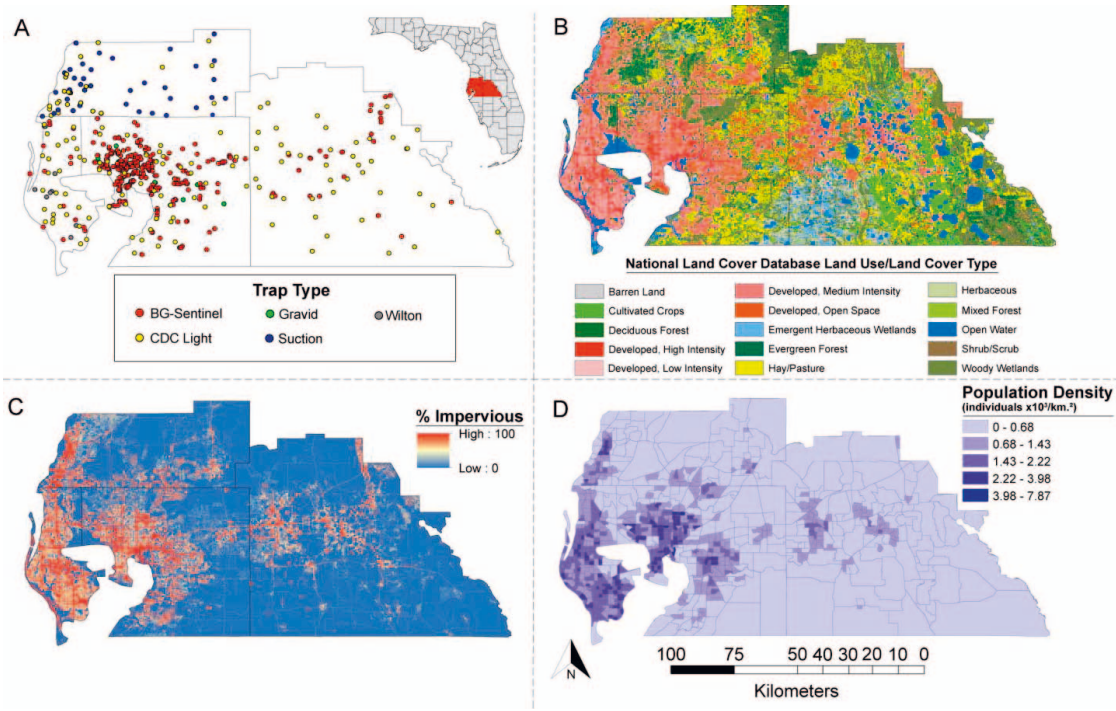

Fig. 1. Distinguishing characteristics related to *Aedes aegypti* in the Tampa Bay area, FL, including (A) location and type of trap, and commonly used predictors (B) land cover and land use, (C) percent imperviousness of built-up environment, and (D) human population density (individuals $\times 10^3$ per km^2).

weighted by collection totals of female *Ae. aegypti* over the 3-year study period.

To accommodate the estimated maximum flight range of *Ae. aegypti*, we created a 500-m buffer around each trap, increasing the likelihood of capturing the overall ecological and physical features of the surrounding environment (Hausermann et al. 1971, Honório et al. 2003, Harrington et al. 2005, Maciel-De-Freitas et al. 2007, Moore and Brown 2022). This buffered region provided locations by which the values of all subsequent model predictors were extracted and averaged for interpretation into the model assessments.

Full information on the habitat modeling predictor datasets is provided in the Supplemental Material Datasets. All processed raster data, aggregated as means within each 500-m-buffered trap location, were exported and merged into a collective dataset. Predictors were evaluated as detailed in Supplemental Table S1. Previous *Ae. aegypti* modeling literature consistently reveals 4 types of predictors as most strongly associated with mosquito habitat: human population density, percent impervious, land use/land cover (LULC), and surface vegetation indices (in particular, normalized difference vegetation index [NDVI] and enhanced vegetation index [EVI]; Fig. 1) (Leisnham et al. 2014, Sallam et al. 2017, Ducheyne et al. 2018, Hamlet et al. 2018, Hopperstad et al. 2021).

Analyses

All statistical analyses were conducted in SAS (version 9.3; SAS Institute Inc., Cary, NC) and JMP (version 16.0.0; SAS Institute Inc., Cary, NC) software. A total of 36 potential model predictors were assessed in modeling female *Ae. aegypti* habitat suitability. Prior to model evaluation, all predictors were tested for multicollinearity (Fig. 2). The EVI and NDVI were further assessed separately by average monthly value. Epidemiologic week trap totals were averaged by county and assessed for unequal variances using Welch's test. Trap group mean totals were analyzed using Tukey's honest significance test (for categorical variables) and generalized linear regression (for continuous variables). Inclusion of parameters within global models was first screened by backward stepwise regression, using minimum Bayesian Information Criterion (BIC) as the stopping rule. Candidate covariates were then analyzed by standard least squares regression. The final model with the lowest overall BIC was selected as the best-fit global model.

Final models were developed for 4 scenarios: 1) Best-fit global model (all submissions from 2017 to 2019 in the Tampa Bay area, FL); 2) Best-fit global model, using only mosquito submissions collected via CDC light traps (the only type used across all 4 counties); 3) Pasco County best-fit model (only using submissions provided by Pasco County from 2020

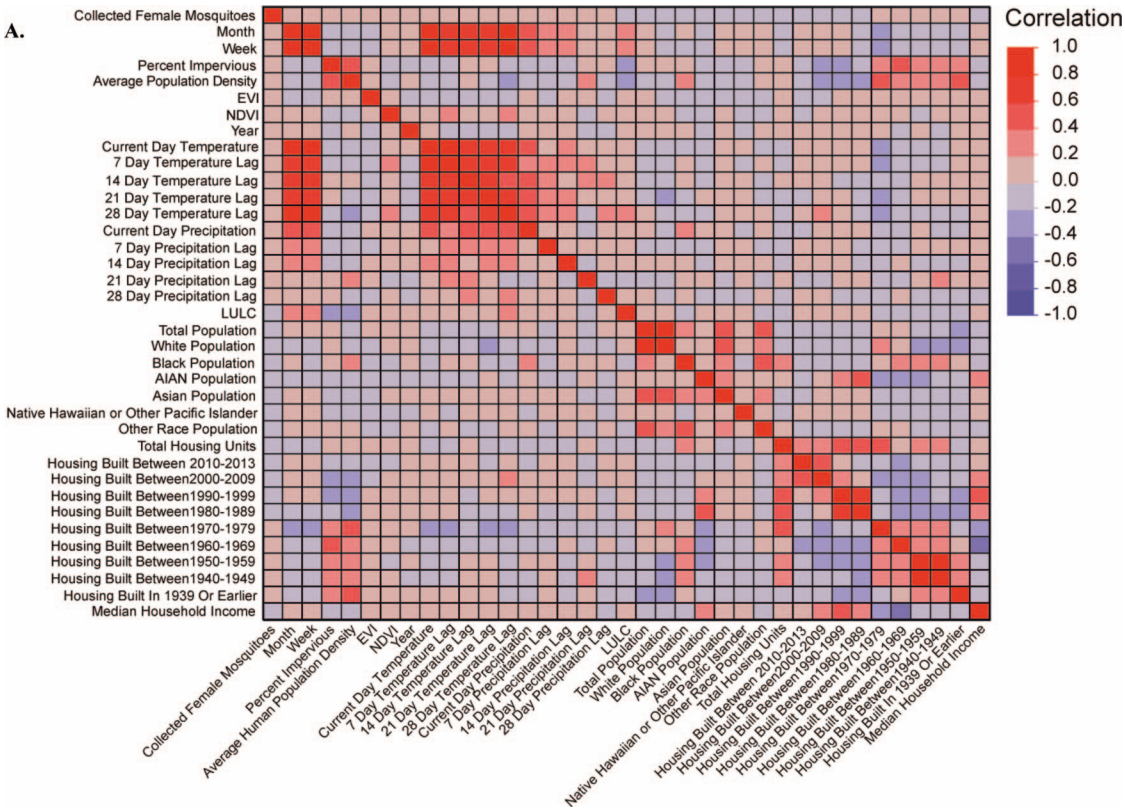

Fig. 2. (A) Color map correlations of all possible model parameters evaluated in this study. (B) Monthly correlations of vegetation spectral responses enhanced vegetation index (EVI) and normalized difference vegetation index (NDVI) are also provided. Values in dark red (≥0.8 correlation) are removed from final model consideration.

collections [PC20]); and 4) PC20 submissions and Tampa Bay area citizen science observations best-fit model.

The 2 best-fit global models (all trap types and only CDC light trap types) were validated using PC20 and citizen science submissions. We used *Ae. aegypti* adults collected from CDC light traps that were placed in new locations within PC20 ($n = 856$ collected mosquitoes; Supplemental Fig. S1A). Research Grade *Ae. aegypti* citizen science observations ($n = 36$; 16 unique locations from 2019 to 2022) from the 4-county region, submitted through iNaturalist.org and acquired from the Global Mosquito Observation Dashboard (http://www.mosquitodashboard.org; Carney et al. 2022), were also applied to model validations (Supplemental Fig. S1B). Overall model strength was assessed by least squares regression of predicted versus actual *Ae. aegypti* abundance.

RESULTS

Entomologic collections by trap

A total of 44,212 female *Ae. aegypti* were collected from 497 traps by the mosquito control agencies of the 4 Tampa Bay counties between 2017 and 2019. Overall, BG-Sentinel traps produced the greatest number of collected mosquitoes ($n = 41,060$). *Aedes aegypti* collections significantly differed by trap type ($P = 0.0342$), with BG-Sentinel producing the greatest average number of collections per trap ($\bar{x} = 130.8$), significantly different from both CDC light ($\bar{x} = 14.8$, $P = 0.0033$) and suction ($\bar{x} = 27.4$, $P = 0.0162$) traps. Average mosquito collections peaked during epidemiologic week 26 and remained high through week 39 (Fig. 3A). These epidemiologic weeks coincide with the summer months of June, July, and August, producing the highest average mosquito collections for all counties and trap types (Table 1). By county, Hillsborough collected the greatest number of mosquitoes both in total and per trap ($\bar{x} = 34.8$), statistically different from the other 3 counties (Pasco, Pinellas, and Polk counties; $\bar{x} = 1.6$, 14.2, and 6.9, respectively; $P < 0.0001$ for each county).

Covariate associations with female *Ae. aegypti* collections

A total of 13 LULC types were present in the Tampa Bay area (Fig. 3B). Mosquito traps placed in developed, low-intensity built environments pro-

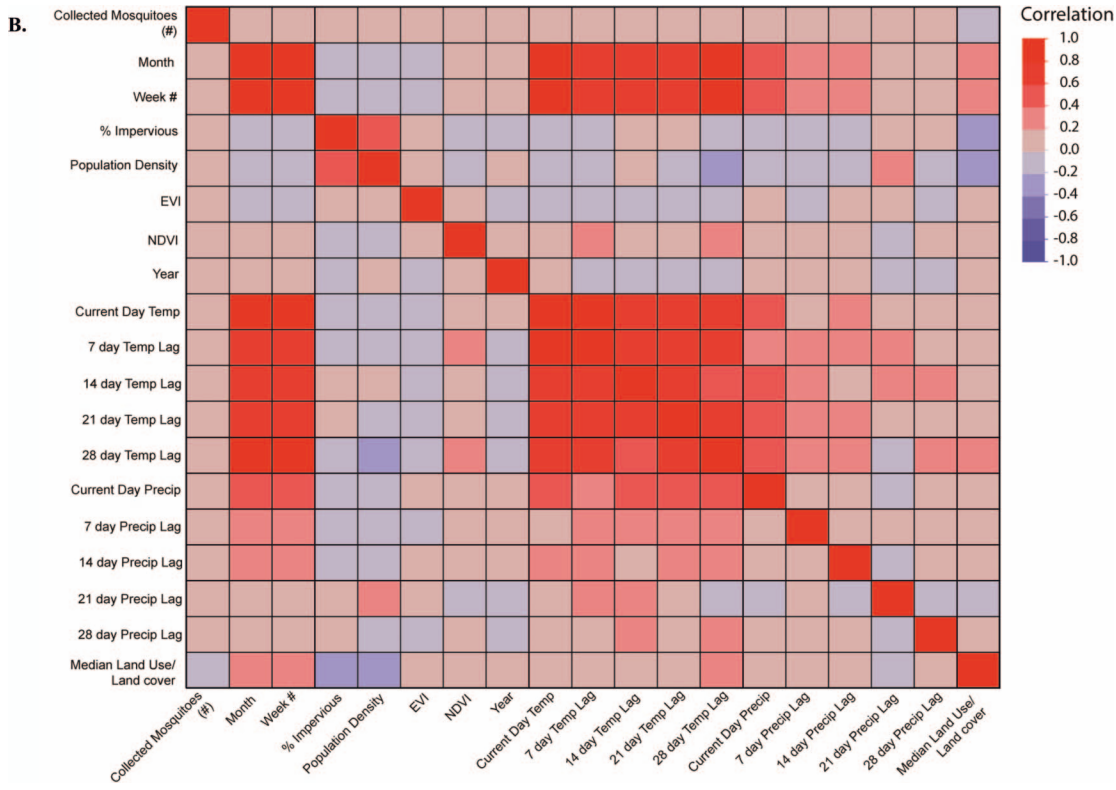

Fig. 2. Continued.

duced the greatest number of female *Ae. aegypti*. Conversely, mosquito traps placed in developed, high-intensity built environments caught the fewest. All other trap types did not differ statistically in the total number of mosquitoes collected. Overall, locations with traps in areas of increasing built environment (e.g., imperviousness and human population density) resulted in significantly greater mosquitoes ($P < 0.0001$; Fig. 3C).

Of the 36 covariates evaluated, temperature-specific variables (e.g., current collection day temperature and 1-, 3-, and 4-wk lags) were 4 of the 5 highest-ranked predictors of *Ae. aegypti* abundance (Table 2). Other notable predictors included total housing units, average human population density, and median household income, all ranked within the top nine in strength of association. Comparatively, EVI had an approximately 3-fold stronger association with weighted *Ae. aegypti* trap collections versus NDVI. However, a breakdown of each vegetation index by month showed similar outcomes in *Ae. aegypti* abundance: the warmest months (August, June, July, and September) produced the greatest trap collections (Table 3).

Habitat modeling and validation

Best-fit global models evaluating the weighted average of all female *Ae. aegypti* collections included 5 covariates: NDVI, year, current day temperature, White population, and median household income ($P < 0.0001$, $R^2 = 0.094$; Table 4). Stratifying the best-fit model to the weighted average of female *Ae. aegypti* collected by CDC light traps maintained 5 distinct covariates ($P < 0.0001$, $R^2 = 0.081$; Table 5): 28-day temperature lag, total housing units, housing built between 1970–79, and housing built between 1960–69. By month, model outputs displayed clustered areas of relatively high- and low-weighted mosquito abundance (indicated by red and blue colors, respectively) that shifted in response to seasonal changes to temperature (Fig. 4).

Validation results of best-fit global models 1 and 2 were as follows: all mosquito trap collections in PC20, $P = 0.11$; CDC light trap–only collections in Pasco County in 2020, $P = 0.19$, $R^2 = 0.03$. Combining the PC20 mosquito collections with the Tampa Bay area citizen science observations resulted in the following: all mosquito trap collections in PC20, $P = 0.11$, $R^2 = 0.054$; CDC light trap-only collections in PC20, $P = 0.16$, $R^2 = 0.031$ (Table 5 and Supplemental Fig. S2).

DISCUSSION

The results of this study demonstrate both the plausibility and practical value of information pro-

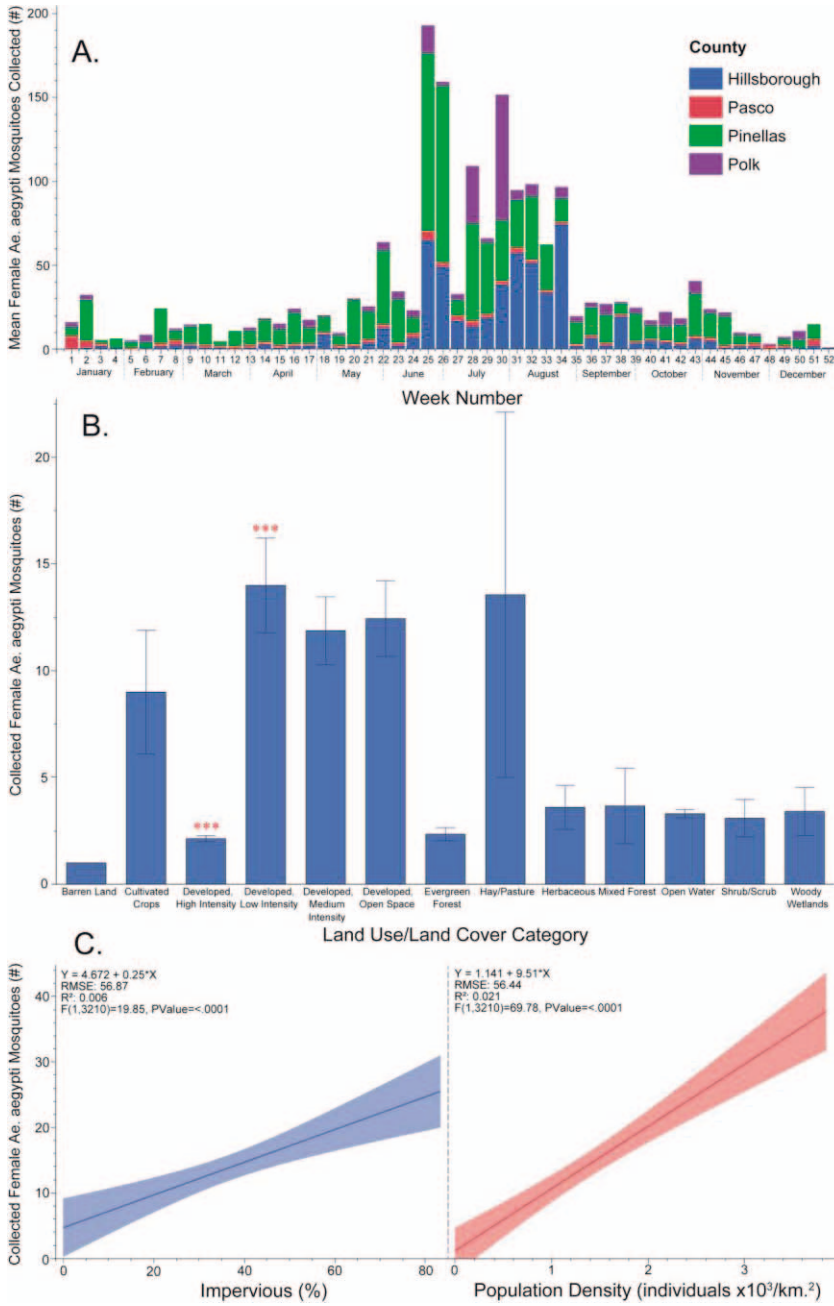

Fig. 3. Average number of female *Aedes aegypti* collected by week from 2017 to 2019. Colors denote (A) unique county of collection, (B) land use/land cover type, and (C) best-fit regressions fit to percent imperviousness of built-up environment (left) and population density (individuals $\times 10^3$ per km^2, right). Error bars represented 1 standard error from the mean. Statistical significance (Student's *t*-test) denoted by asterisks (*** = $P < 0.0001$).

vided by *Ae. aegypti* abundance models. All predictors assessed in this study are free and publicly available. With the exception of NDVI and EVI, all data are analysis-ready, requiring no additional processing or preparation for use. Our methodology and results are consistent with those of previous literature on assessing vector mosquito risk, in highlighting the importance of utilizing climatic data, particularly mean temperature and its associated weekly lags (Uelmen et al. 2021). Also important are socioeconomic, race, and household age predictors in *Ae. aegypti* risk assessments (Little et al. 2017,

Table 2. Predictor estimates and overall rank for all covariates in study (*Bootstrap Forest* partitioning, 100 trees).

Predictor	Contribution	Portion	Rank
7-day temperature lag	874,117	0.2022	1
21-day temperature lag	351,198	0.0812	2
28-day temperature lag	342,133	0.0792	3
Total housing units	268,500	0.0621	4
Current day temperature	264,536	0.0612	5
Average human population density	249,854	0.0578	6
Current day precipitation	209,952	0.0486	7
Enhanced vegetation index	171,098	0.0396	8
Median household income	161,265	0.0373	9
21-day precipitation lag	154,749	0.0358	10
14-day temperature lag	121,643	0.0281	11
14-day precipitation lag	90,424	0.0209	12
Land use/land cover	77,973	0.0180	13
Housing built between 1970–79	74,448	0.0172	14
Housing built between 1950–59	74,387	0.0172	15
Housing built between 1990–99	69,669	0.0161	16
Percent impervious	68,424	0.0158	17
7-day precipitation lag	67,692	0.0157	18
Housing built between 2000–09	65,832	0.0152	19
Week no.	64,463	0.0149	20
Month	63,632	0.0147	21
Normalized difference vegetation index	58,530	0.0135	22
White population	55,265	0.0128	23
28-day precipitation lag	50,183	0.0116	24
Housing built between 1980–89	46,655	0.0108	25
Year	41,815	0.0097	26
Housing built in 1939 or earlier	40,325	0.0093	27
Black population	31,670	0.0073	28
Housing built between 1960–69	31,403	0.0073	29
Housing built between 1940–49	30,230	0.0070	30
Other race population	14,548	0.0034	31
Total population	13,816	0.0032	32
Asian population	13,592	0.0031	33
Housing built between 2010–13	8,462	0.0020	34
Native Hawaiian or other Pacific Islander	31	0.0000	35
American Indian and Alaska Native population	23	0.0000	36

Table 3. Landcover spectral responses for enhanced vegetation index (EVI) and normalized difference vegetation index (NDVI) by month parameters and rank.

Predictor	Contribution	Portion	Rank
EVI			
Aug	1,111,957	0.636	1
Jun	236,400	0.1352	2
Jul	146,464	0.0838	3
Sep	93,807	0.0537	4
Jan	93,515	0.0535	5
Mar	49,585	0.0284	6
Nov	10,291	0.0059	7
Apr	2,093	0.0012	8
May	2,032	0.0012	9
Oct	1,059	0.0006	10
Feb	901	0.0005	11
Dec	138	0.0001	12
NVDI			
Aug	1,856,857	0.7124	1
Jun	373,371	0.1433	2
Jul	127,171	0.0488	3
Sep	98,725	0.0379	4
Jan	80,691	0.031	5
Mar	51,902	0.0199	6
Nov	11,626	0.0045	7
May	2,190	0.0008	8
Apr	2,150	0.0008	9
Feb	1,018	0.0004	10
Oct	576	0.0002	11
Dec	146	0.0001	12

Goodman et al. 2018). Previous literature has established one or more of these predictors as valuable in mosquito ecology, but rarely do these nonenvironmental forces occupy >50% of a final model's total covariate composition (Karki et al. 2020).

Another key finding is the importance of quality and spatiotemporal resolution of data. The 4-county global models assessed in this study were significant, but contained greater root mean square errors, higher model assessment criterion (AICc; Akaike information criterion corrected) and BIC (Bayesian information criterion), and poorer mean fit (as indicated by R^2) compared with the smaller models in Table 5. Despite far lower sample sizes than the 4 county assessments, both best-fit models were strongly significant (2020 Pasco County collections alone as well as paired with citizen science observations; $P = 0.0001$ and $P = 0.0009$, respectively). Out of all best-fit and validation models analyzed, the best-fit 2020 Pasco County collections had the strongest correlation ($R^2 = 0.124$) and lowest model assessment criterion (AICc = 1,058.21, BIC = 1,073.12).

While all predictors herein are freely available to the public, these models cater to mosquito control agencies and require mosquito abundance data as the primary independent variable. Additionally, NDVI and EVI do require a modest computational skillset. To alleviate that burden to novice users, we provide the publicly available websites where these layers can be acquired, as well as a copy of all raw and processed imagery (https://drive.google.com/file/d/1_2QHlHqYVDYTKwmXtsHN87Y3ftkNZWq7). Fortunately, at least for the Tampa Bay area, high-quality abundance models can be generated without the use of any vegetation indices, although this is likely highly variable and specific to geography, time, and species of interest. Results from this analysis demonstrate that simplified models—that is, data layers consisting of at least one temperature

Table 4. Best-fit global model report for *Aedes aegypti* in the Tampa Bay area, FL.

Summary of fit	
RSquare	0.0937
RSquare adj	0.0887
Root mean square error	70.82
Mean of response	20.48
Observations (or sum wgts)	925
AICc	10514.38
BIC	10548.07

Analysis of variance				
Source	**DF**	**Sum of squares**	**Mean square**	**F ratio**
Model	5	476307.8	95261.6	18.99
Error	919	4609127.1	5015.4	
C. total	924	5085434.9		
P value	<0.0001			

Parameter estimates				
Term	**Estimate**	**SE**	**t ratio**	**Prob > |t|**
Intercept	6538.42	3055.91	2.14	0.0326
NDVI	-0.0037	0.0013	-2.77	0.0056
Year	-3.27	1.52	-2.16	0.0314
Current day temperature	4.95	0.64	7.69	<0.0001
White population	-0.090	0.027	-3.27	0.0011
Median household income	-0.00055	0.00013	-4.25	<0.0001

Parameter effects					
Source	**Nparm**	**DF**	**Sum of squares**	**F ratio**	**Prob > F**
NDVI	1	1	38609.56	7.70	0.0056
Year	1	1	23291.68	4.64	0.0314
Current day temperature	1	1	296431.48	59.10	<0.0001
White population	1	1	53701.10	10.71	0.0011
Median household income	1	1	90484.39	18.04	<0.0001

lag (7, 21, and/or 28 days), one socioeconomic (number of housing units), and one demographic (population density) variable—produce surprisingly robust estimates of mosquito abundance that can be used as stratified approximations for exposure risk.

All statistical models are inherently error-prone and do not capture all details of reality. That being said, a useful model is a good model. Limitations of the data and methodology used in our assessment include the fact that our independent variable, weighted *Ae. aegypti* abundance by trap location, is a presence-only event, and therefore the inclusion of absence data may strengthen the model output. Our modeling approach incorporated annual, monthly, and weekly data at varying resolutions. As a general guide, higher resolutions in both space and time are preferable (Little et al. 2017). Overall, our spatial resolution ranged from 4 km (PRISM climate data) to 30 m (impervious and LULC). Lastly, we produced monthly model abundance maps as a visual guide for our readers. Following suit with the prior example, higher temporal resolutions would be more useful for mosquito control personnel, and the maps herein could be modified to produce weekly results, for example.

A key advantage of the 4 counties assessed was the longstanding operation of dedicated mosquito control agencies. However, each agency deploys their own methods for surveillance and control, including unique protocols that prompt action. These differences result in inconsistencies in final data collections (frequency, trap type and locations) and likely yield weaker model fits for a multicounty conglomerate model compared to individual county models

Our results mirror similar findings (Leisnham et al. 2014) by demonstrating an overall peak abundance trend during the hottest months in the Tampa Bay area (June–September), when temperatures consistently reach a high in the 90s (°F) (>32°C) and occasionally reach 100s (°F) (>37°C). These temperatures exceed reported thermal maximums for both dengue and Zika viruses within *Ae. aegypti* (Shocket et al. 2020). Additional studies should investigate the thermal limitations of arboviruses within *Ae. aegypti* to assess seasonal disease activity (Monaghan et al. 2019), including the plausibility that overall transmission may decrease, while overall mosquito abundance may increase.

As expected, the predictors included in our final models are those strongly associated with temperature and human-built environment (Leisnham and Juliano 2009, Leandro-Reguillo et al. 2017). In general, locations that were more urban (and thus have higher population densities) with older homes tend to have the highest predicted mosquito abundances. Of the 4

Table 5. Comparison of all best-fit and validation model combinations assessed for *Aedes aegypti* abundance in the Tampa Bay, FL, area.[1]

Model	Covariates	*P*	R^2	RMSE	AICc	BIC	Figure reference
Best-fit global model 1 (all submissions 2017–19, Tampa Bay, FL, area)	NDVI, year, current day temperature, white population, median household income	<0.0001	0.094	70.82	10,514.38	10,548.07	S2A (top left)
Best-fit global model 2 (all submissions collected via CDC light traps only, 2017–19)	28-day temperature lag, total housing units, housing built between 1970–79, housing built between 1960–69	<0.0001	0.081	6.31	3,593.52	3,619.23	S2A (top right)
Pasco best fit (PC20 submissions only[2])	7-day temperature lag, current day precipitation, AIAN population	0.0001	0.124	6.75	1,058.21	1,073.12	S2A (bottom left)
Pasco + citizen science best fit (all 2020 Tampa Bay, FL, area submissions)	Current day precipitation	0.0009	0.051	6.37	1,397.52	1,407.49	S2A (bottom right)
Validation of model 1 (using only PC20 submissions)	7-day temperature lag, current day precipitation, AIAN population	0.11	0.056	7.05	1,074.27	1,094.96	S2B (top left)
Validation of model 2 (using only PC20 submissions)	Current day precipitation	0.19	0.03	6.58	1,308.9	1,328.16	S2B (bottom left)
Validation of model 1 (PC20 and citizen science submission)[3]	NDVI, year, current day temperature, White population, median household income	0.11	0.054	7.02	1,133.38	1,154.5	S2B (top right)
Validation of model 2 (PC20 and citizen science submission)	28-day temperature lag, total housing units, housing built between 1970–79, housing built between 1960–69	0.16	0.031	6.48	1,408.14	1,427.9	S2B (bottom right)

[1] AICc, Akaike Information Criterion corrected; BIC, Bayesian Information Criterion; CDC, Centers for Disease Control and Prevention; AIAN, American Indian and Alaska Native population; NDVI, normalized difference vegetation index; RMSE, root mean square error.
[2] PC20, Pasco County 2020 submissions.
[3] Models validated with all PC20 collections ($n = 856$) and Tampa Bay, FL, area citizen science submissions ($n = 36$).

counties, Pinellas had the highest abundance of *Ae. aegypti* per trap as a proportion of the total county area. Pinellas also has the greatest mean population density among the 4 counties. Conversely, Polk County, the most rural and least densely populated county out of the four, had the overall lowest mosquito abundance. However, the location of highest abundance shifts to downtown Tampa and its immediate suburbs in the summer months, which has public health implications for the residents there.

Citizen science has enormous potential for vector monitoring going forward (Palmer et al. 2017, Carney et al. 2022). If current monitoring trends are mostly trap-based, then there is the potential for spatial gaps in our understanding of new extents of invasive or expanding arbovirus vectors. For example, a citizen science monitoring project recently yielded the first iNaturalist observations of *Ae. vittatus* (Bigot) globally and *Ae. scapularis* (Rondani) in the USA (Carney et al. 2022). These 2 species in particular, along with *Ae. aegypti* in the Tampa Bay area for the present study, were the 3 targets of the campaign (mosquitoAI.org). Our analyses herein took advantage of 36 Research Grade observations of *Ae. aegypti* from 16 unique locations within the study area, providing a litmus test for our models' overall performance and robustness. Ideally, increasing the number of citizen science observations could improve the data needed to conduct even more generalizable models.

Due to the strong association of *Ae. aegypti* with urban and suburban landscapes, combined with a relatively short flight range (500 m) of the mosquito, *Ae. aegypti*–borne viruses are primarily an urban threat. Warming climates and range expansion (Kamal et al. 2018) necessitate updating urban risk models to include additional latitudes within theoretical suitability of *Ae. aegypti*. Lastly, ports of entry are vital in facilitating *Ae. aegypti* introductions. Given that the Miami Zika outbreak originated a few miles from the Miami International Airport (Gardner et al. 2017, Marini et al. 2017), future efforts should

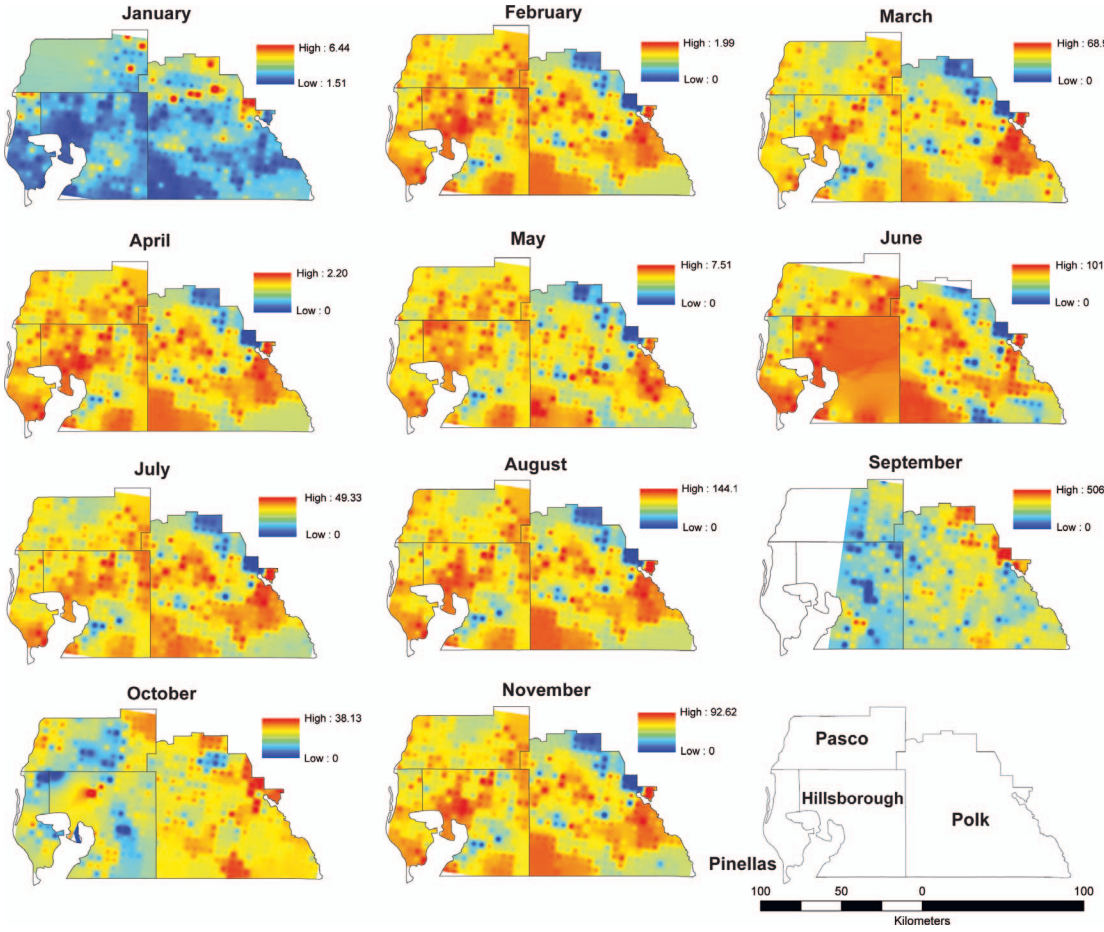

Fig. 4. Best-fit global models output estimating mosquito abundances of *Aedes aegypti* in the Tampa Bay, FL, area by month. Due to a lack of submissions ($n = 19$) for the month of December, model output could not be produced.

examine the distance of high-risk areas to possible *Ae. aegypti* introduction sources, including various ports of entry. For example, Leandro-Reguillo et al. (2017) examined the potential for Zika virus transmission to proliferate in Barcelona, and of the 3 highest risk areas determined, one (Old Town) is near the port of Barcelona. Looking forward, technological advances will continue to greatly assist mosquito surveillance and control activities. From high-resolution imagery remotely sensed from space to mobile device-based mosquito observations on the ground, such technologies can be leveraged for the prediction, detection, and monitoring of invasive vectors, and ultimately help to combat mosquito-borne diseases well into the future.

SUPPLEMENTAL MATERIAL

Supplemental material is available online with the article.

ACKNOWLEDGMENTS

This research was funded by the National Science Foundation under Grant No. IIS-2014547 to R.M.C.

REFERENCES CITED

Beeman SP, Morrison AM, Unnasch TR, Unnasch RS. 2021. Ensemble ecological niche modeling of West Nile virus probability in Florida. *PLoS ONE* 8:16. https://doi.org/10.1371/journal.pone.0256868

Carney R, Mapes C, Low R, Long A, Bowser A, Durieux D, Rivera K, Dekramanjian B, Bartumeus F, Guerrero D, Seltzer C, Azam F, Chellappan S, Palmer JP. 2022. Integrating global citizen science platforms to enable next-generation surveillance of invasive and vector mosquitoes. *Insects* 13:675. https://doi.org/10.3390/insects13080675

CDC [Centers for Disease Control and Prevention]. 2017. *Potential range of* Aedes aegypti *and* Aedes albopictus *in the United States* [Internet]. Atlanta, GA: Centers for

Disease Control and Prevention [accessed December 18, 2022].
CDC [Centers for Disease Control and Prevention]. 2022. *Dengue cases in the US* [Internet]. Atlanta, GA: Centers for Disease Control and Prevention, National Center for Emerging and Zoonotic Infectious Diseases (NCEZID), Division of Vector-Borne Diseases (DVBD) [accessed December 18, 2022]. Available from: https://www.cdc.gov/dengue/statistics-maps/2022.html.
Donnelly JW. 1993. *Aedes aegypti* in New Jersey. *J Am Mosq Control Assoc* 9:238.
Ducheyne E, Minh NNT, Haddad N, Bryssinckx W, Buliva E, Simard F, Malik MR, Charlier J, de Waele V, Mahmoud O, Mukhtar M, Bouattour A, Hussain A, Hendrickx G, Roiz D. 2018. Current and future distribution of *Aedes aegypti* and *Aedes albopictus* (Diptera: Culicidae) in WHO Eastern Mediterranean Region. *Int J Health Geogr* 17:4. https://doi.org/10.1186/s12942-018-0125-0
FDH [Florida Department of Health]. 2021. *Dengue occurrence in Florida*. Tallahassee, FL: Florida Department of Health.
Gardner L, Chen N, Sarkar S. 2017. Vector status of *Aedes* species determines geographical risk of autochthonous Zika virus establishment. *PLoS Negl Trop Dis* 11:e0005487. https://doi.org/10.1371/journal.pntd.0005487
Goodman H, Egizi A, Fonseca DM, Leisnham PT, LaDeau SL. 2018. Primary blood-hosts of mosquitoes are influenced by social and ecological conditions in a complex urban landscape. *Parasit Vectors* 11:218. https://doi.org/10.1186/s13071-018-2779-7
Hamlet A, Jean K, Perea W, Yactayo S, Biey J, van Kerkhove M, Ferguson N, Garske T. 2018. The seasonal influence of climate and environment on Yellow fever transmission across Africa. *PLoS Negl Trop Dis* 12:e0006284. https://doi.org/10.1371/journal.pntd.0006284
Harrington LC, Scott TW, Lerdthusnee K, Coleman RC, Costero A, Clark GG, Jones JJ, Kitthawee S, Kittayapong P, Sithiprasasna R, Edman JD. 2005. Dispersal of the dengue vector *Aedes aegypti* within and between rural communities. *Am J Trop Med Hyg* 72:209–220. https://doi.org/10.4269/ajtmh.2005.72.209
Hartz B. 2022. *Tampa Bay among fastest-growing large US metro areas* [Internet]. Sarasota, FL: Business Observer Florida [accessed December 20, 2022]. Available from: https://www.businessobserverfl.com/news/2022/dec/23/tampa-bay-among-fastest-growing-large-u-s-metro-areas/.
Hausermann W, Fay RW, Hacker CS. 1971. Dispersal of genetically marked female *Aedes aegypti* in Mississippi. *Mosq News* 31:37–51.
Honório NA, da Costa Silva W, Leite PJ, Gonçalves JM, Lounibos LP, Lourenço-de-Oliveira R. 2003. Dispersal of *Aedes aegypti* and *Aedes albopictus* (Diptera: Culicidae) in an urban endemic Dengue area in the state of Rio de Janeiro, Brazil. *Mem Inst Oswaldo Cruz* 98:191–198. https://doi.org/10.1590/S0074-02762003000200005
Hopperstad KA, Sallam MF, Reiskind MH. 2021. Estimations of fine-scale species distributions of *Aedes aegypti* and *Aedes albopictus* (Diptera: Culicidae) in eastern Florida. *J Med Entomol* 58:699–707. https://doi.org/10.1093/jme/tjaa216
Huang CC, Tam TYT, Chern YR, Lung SCC, Chen NT, Wu C. 2018. Spatial clustering of dengue fever incidence and its association with surrounding greenness. *Int J Environ Res Public Health* 15:1869. https://doi.org/10.3390/ijerph15091869
Kamal M, Kenawy MA, Rady MH, Khaled AS, Samy AM. 2018. Mapping the global potential distributions of two arboviral vectors *Aedes aegypti* and *Ae. albopictus* under changing climate. *PLoS One* 13:e0210122. https://doi.org/10.1371/journal.pone.0210122
Karki S, Brown WM, Uelmen J, Ruiz MO, Smith RL. 2020. The drivers of West Nile virus human illness in the Chicago, Illinois, USA area: fine scale dynamic effects of weather, mosquito infection, social, and biological conditions. *PLoS One* 15:e0227160. https://doi.org/10.1371/journal.pone.0227160
Kraemer MUG, Reiner RC, Brady OJ, Messina JP, Gilbert M, Pigott DM, Yi D, Johnson K, Earl L, Marczak LB, Shirude S, Weaver ND, Bisanzio D, Perkins TA, Lai S, Lu X, Jones P, Coelho GE, Carvalho RG, Van Bortel W, Marsboom C, Hendrickx G, Schaffner F, Moore CG, Nax HH, Bengtsson L, Wetter E, Tatem AJ, Brownstein JS, Smith DL, Lambrechts L, Cauchemez S, Linard C, Faria NR, Pybus OG, Scott TW, Liu Q, Yu H, Wint GRW, Hay SI, Golding N. 2019. Past and future spread of the arbovirus vectors *Aedes aegypti* and *Aedes albopictus*. *Nat Microbiol* 4:854–863. https://doi.org/10.1038/s41564-019-0376-y
Kraemer MUG, Sinka ME, Duda KA, Mylne A, Shearer FM, Brady OJ, Messina JP, Barker CM, Moore CG, Carvalho RG, Coelho GE, van Bortel W, Hendrickx G, Schaffner F, Wint GRW, Elyazar IRF, Teng HJ, Hay SI. 2015a. The global compendium of *Aedes aegypti* and *Ae. albopictus* occurrence. *Sci Data* 2:150035. https://doi.org/10.1038/sdata.2015.35
Kraemer MUG, Sinka ME, Duda KA, Mylne AQN, Shearer FM, Barker CM, Moore CG, Carvalho RG, Coelho GE, Van Bortel W, Hendrickx G, Schaffner F, Elyazar IRF, Teng HJ, Brady OJ, Messina JP, Pigott DM, Scott TW, Smith DL, Wint GRW, Golding N, Hay SI. 2015b. The global distribution of the arbovirus vectors *Aedes aegypti* and *Ae. albopictus. Elife* 4:e08347. https://doi.org/10.7554/eLife.08347
Leandro-Reguillo P, Panaou T, Carney R, Jacob BG. 2017. Fuzzification of multi-criteria proxy geoclassifiable vegetation and landscape biosignature estimators to predict the potential invasion of *Aedes aegypti* in Barcelona, Spain. *Int J Geogr Inf* 4:1–19.
Leisnham PT, Juliano SA. 2009. Spatial and temporal patterns of coexistence between competing *Aedes* mosquitoes in urban Florida. *Oecologia* 160:343–352. https://doi.org/10.1007/s00442-009-1305-1
Leisnham PT, LaDeau SL, Juliano SA. 2014. Spatial and temporal habitat segregation of mosquitoes in urban Florida. *PLoS One* 9:e91655. https://doi.org/10.1371/journal.pone.0091655
Likos A, Griffin I, Bingham AM, Stanek D, Fischer M, White S, Hamilton J, Eisenstein L, Atrubin D, Mulay P, Scott B, Jenkins P, Fernandez D, Rico E, Gillis L, Jean R, Cone M, Blackmore C, McAllister J, Vasquez C, Rivera L, Philip C. 2016. Local mosquito-borne transmission of Zika virus—Miami-Dade and Broward Counties, Florida, June–August 2016. *MMWR Morb Mortal Wkly Rep* 65:1032–1038. https://doi.org/10.15585/mmwr.mm6538e1
Little E, Biehler D, Leisnham PT, Jordan R, Wilson RS, LaDeau SL. 2017. Socio-ecological mechanisms supporting high densities of *Aedes albopictus* (Diptera:

Culicidae) in Baltimore, MD. *J Med Entomol* 54:1183–1192. https://doi.org/10.1093/jme/tjx103

Maciel-De-Freitas R, Codeço CT, Lourenço-De-Oliveira R. 2007. Body size-associated survival and dispersal rates of *Aedes aegypti* in Rio de Janeiro. *Med Vet Entomol* 21:284–292. https://doi.org/10.1111/j.1365-2915.2007.00694.x

Marini G, Guzzetta G, Rosà R, Merler S. 2017. First outbreak of Zika virus in the continental United States: a modelling analysis. *Euro Surveill* 22:30612. https://doi.org/10.2807/1560-7917.ES.2017.22.37.30612

Monaghan AJ, Schmidt CA, Hayden MH, Smith KA, Reiskind MH, Cabell R, Ernst KC. 2019. A simple model to predict the potential abundance of *Aedes aegypti* mosquitoes one month in advance. *Am J Trop Med Hyg* 100:434–437. https://doi.org/10.4269/ajtmh.17-0860

Moore TC, Brown HE. 2022. Estimating *Aedes aegypti* (Diptera: Culicidae) flight distance: meta-data analysis. *J Med Entomol* 59:1164–1170. https://doi.org/10.1093/jme/tjac070

Palmer JRB, Oltra A, Collantes F, Delgado JA, Lucientes J, Delacour S, Bengoa M, Eritja R, Bartumeus F. 2017. Citizen science provides a reliable and scalable tool to track disease-carrying mosquitoes. *Nat Commun* 8:916. https://doi.org/10.1038/s41467-017-00914-9

Patterson J, Sammon M, Garg M. 2016. Dengue, Zika and Chikungunya: emerging arboviruses in the New World. *West J Emerg Med* 17:671–679. https://doi.org/10.5811/westjem.2016.9.30904

Reeves LE, Sloyer KE, Tyler-Julian K, Heinig R, Rosales A, Domingo C, Burkett-Cadena ND. 2023. *Culex* (*Phenacomyia*) *lactator* (Diptera: Culicidae) in southern Florida, USA: a new subgenus and species country record. *J Med Entomol* tjad023 [published online ahead of print March 22, 2023]. Available from: https://doi.org/10.1093/jme/tjad023

Rey JR. 2014. Dengue in Florida (USA). *Insects* 5:991–1000. https://doi.org/10.3390/insects5040991

Sallam MF, Fizer C, Pilant AN, Whung PY. 2017. Systematic review: land cover, meteorological, and socioeconomic determinants of *Aedes* mosquito habitat for risk mapping. *Int J Environ Res Public Health* 14:1230. https://doi.org/10.3390/ijerph14101230

Shocket MS, Verwillow AB, Numazu MG, Slamani H, Cohen JM, el Moustaid F, Rohr J, Johnson LR, Mordecai EA. 2020. Transmission of West Nile and five other temperate mosquito-borne viruses peaks at temperatures between 23°C and 26°C. *Elife* 9:e58511. https://doi.org/10.7554/ELIFE.58511

Takken W, Verhulst NO. 2013. Host preferences of blood-feeding mosquitoes. *Annu Rev Entomol* 58:433–453. https://doi.org/10.1146/annurev-ento-120811-153618

Uelmen JA, Irwin P, Brown WM, Karki S, Ruiz MO, Li B, Smith RL. 2021. Dynamics of data availability in disease modeling: an example evaluating the tradeoffs of ultra-fine-scale factors applied to human West Nile virus disease models in the Chicago area, USA. *PLoS One* 16:e0251517. https://doi.org/10.1371/journal.pone.0251517

WHO [World Health Organization]. 2021. *Dengue and severe dengue*. Geneva, Switzerland: World Health Organization.

Wilder-Smith A, Ooi EE, Horstick O, Wills B. 2019. Dengue. *Lancet* 393:350–363. https://doi.org/10.1016/S0140-6736(18)32560-1

SUPPLEMENTARY MATERIALS

for

A HABITAT MODEL FOR DISEASE VECTOR *AEDES AEGYPTI*
IN THE TAMPA BAY AREA, FLORIDA

DATASETS

With the exception of the *Aedes* (*Ae*.) *aegypti* abundance data provided by the four mosquito control agencies, all datasets used in this study are freely available to the public.

Citizen Science Mosquito Submissions:
www.mosquitodashboard.org

- Interactive dashboard for users to select data on selectable filters, including genus and species, by date and location (Carney et al., 2022).

Land Use Land Cover (LULC):
https://www.mrlc.gov/

- An additional landscape-level predictor of *Ae. aegypti* habitat is LULC, providing a categorical response describing the type of land in a given pixel. The LULC data (30-meter resolution) used was the 2019 version provided by the National Land Cover Database (NLCD) (https://www.mrlc.gov/). LULC data was extracted using the S*patial Join* tool in ArcMap, selecting the mean value response for each 500-meter buffer trap location.

Imperviousness:
https://www.mrlc.gov/

- This data is provided by the NLCD (2019) and has a resolution of 30 m. An additional metric strongly associated with the built environment is the lack of reflective infrared (band 4) and red (band 3) wavelengths. Ranging from 0 (high vegetation reflectance) to 1 (no vegetation reflectance), imperviousness is best characterized by materials that eliminate or hinder vegetative growth, often referring to characteristics of human development like asphalt, concrete, buildings, pavement, trails, etc. Given that *Ae. aegypti* prefers habitat that is strongly associated with humans, imperviousness provides an additional metric that differs from categorical LULC information.

Human Population (Density):
https://data.census.gov/table?d=ACS+5-Year+Estimates+Data+Profiles&tid=ACSDP5Y2019.DP05&hidePreview=false

- Demographic information was retrieved from census tract-level US Census Bureau (U.S. Census Bureau, 2019). Census tracts provide comparable population sizes, but across varied land area sizes. As a result, population density can be approximated by dividing the total population (census-reported number of individuals) by area ($km.^2$).

Household Income (Median):
https://data.census.gov/table?q=B19013&g=0400000US12$1400000&tid=ACSDT5Y2020.B19013

- Data was acquired at the census tract level by the American Community Survey's 2020 one-year estimate of the past 12 months of income, in 2020 inflation-adjusted dollars (U.S. Census Bureau, 2020b).

Housing Age:
https://data.census.gov/table?tid=ACSDP1Y2021.DP04

- Housing age, a proxy for community development and physical characteristics, was provided by the American Community Survey's 2021 one-year estimate (U.S. Census Bureau, 2021). Houses by each census tract were aged based on 10-year bins starting from 2020 or later, 2019-2010, 2009-2000, etc. until 1939 or earlier.

Race & Ethnicity:
https://data.census.gov/table?q=P1:+RACE&tid=DECENNIALPL2020.P1&hidePreview=true

- Block-level estimates for the 2020 racial and ethnic demographic makeup of residents was acquired by the U.S. Census Bureau, 2020 Census Redistricting Data (U.S. Census Bureau, 2020a). Racial demographics represented in the Tampa Bay area were classified as: American Indian or Alaska Native (AIAN), Asian, Black, Native Hawaiian and Other Pacific Islander, Other Race, and White.

Climate:
https://prism.oregonstate.edu/normals/

- Daily mean temperature (ºC) and total precipitation (mm.) raster images were provided by the PRISM climate group (Northwest Alliance for Computational Science and Engineering at Oregon State University: https://prism.oregonstate.edu/normals/). Each image provides interpolated values for the contiguous United States at 4-km pixel resolution. To increase processing time, each raster image was reduced to only the four-county Tampa Bay region using the E*xtract by Mask* tool in ArcMap. Each daily temperature and precipitation raster was then aggregated by each 500 m buffered trap location using the *Zonal Statistics as Table* tool. All pixels contained within each buffered location were averaged.

Vegetation Indices:
https://drive.google.com/file/d/1_2QHlHqYVDYTKwmXtsHN87Y3ftkNZWq7

- Each vegetation index was created using 30-meter resolution Landsat 8 satellite data (Collection 2 Level-2) for the year 2019 accessed via the United States Geological Survey (USGS) EarthExplorer portal (https://earthexplorer.usgs.gov/). Each satellite raster comprised four spectral bands: red (619–651 nm), green (525–585 nm), blue (435–495 nm), and near infrared (808–882 nm). EVI and NDVI were created using the R*aster Calculator* tool in ArcMap (Esri) (Landsat Missions, 2023; Nagler et al., 2005; Purevdorj et al., 1998). To maximize the likelihood that each 30-meter pixel has satellite coverage, monthly composite images were generated by averaging calculated index values using all available processed images for each respective county. This provided near 100%

spatiotemporal coverage with little to no cloud cover for all pixels, except for September (coverage approximately 50%), due to consistently heavy cloud interference for all available images. The values for each final vegetation index raster were extracted for all 500-meter trap locations using the S*patial Join* tool in ArcMap.

Satellite Imagery Metadata:

- All data is available for free from https://earthexplorer.usgs.gov/
- Data provided in github repository are all available Landsat 8 images (collection 2 level 2 processed) with <30% cloud cover that cover some or all of the four county Tampa Bay region from January 1, 2019 to June 30, 2019
- Each available image was aggregated by month and analyzed as a composite image. If one or more layers overlapped for any given month, the pixels were averaged.
- These images can be imported directly into the software application of choice for calculating NDVI, EVI, or any other vegetative or spectral response desired.

Table S1. Summary of geospatial processing of predictors used in this study. All spatial data was processed in ArcMap, then exported for statistical analysis in SAS and JMP programs. Final model parameters were then integrated back into ArcMap to generate prediction maps and final model validation outputs.

Purpose	Layers Used			Geoprocessing Tool				Outcome
	Layer 1: Type	*Layer 2: Type*	*Layer 3: Type*	*Step 1*	*Step 2*	*Step 3*	*Step 4*	
Create buffered regions around each trap location	Trap locations (point shapefile)			Buffer (Geoprocessing Toolbar)				500 m circled buffer around each trap point (polygon shapefile)
Extract satellite pixel data	Four-county Tampa Bay, FL (polygon shapefile)	Raster satellite images (i.e. daily precipitation or temperature, vegetation reflectance)	Buffered trap location (polygon shapefile)	Extract by Mask (Spatial Analyst)	Zonal Statistics as Table (Spatial Analyst) using buffered trap polygons			Generate summarized values of interest (i.e. mean % impervious) by 500 m buffered polygon
Create vegetation indices	Four-band Landsat 8 image (raster)			Raster Calculator (Spatial Analyst)	Use Equation 1 (EVI) or Equation 2 (NDVI)			Single band raster image of calculated spectral signature of EVI or NDVI by pixel
Create model prediction maps	28-day temperature lag (raster)	14-day Precipitation Lag (raster)	EVI and/or NDVI (raster)	Export summary table of each raster (by 500 m. polygon shapefile)	Create master data analysis table, analyze best-fit model (conducted in SAS)	Use original high-resolution pixel raster image of each included final model parameter	Input parameter specific values of best-fit model using raster calculator (Spatial Analyst)	Generate pixel values based on best-fit model predictions
Validate models	2020 Pasco County traps (point shapefile)	28 day Temperature Lag, 14 day Precipitation Lag (raster)		Extract by Mask (Spatial Analyst)	Input parameter specific best-fit model values using raster calculator (Spatial Analyst)	Subtract 2020 model with original best-fit pixel values using raster calculator (Spatial Analyst)	Conduct statistical analyses and display x,y point values for regressions	Provides statistical comparison of pixel "agreement" between best-fit models based on retrospective data

A

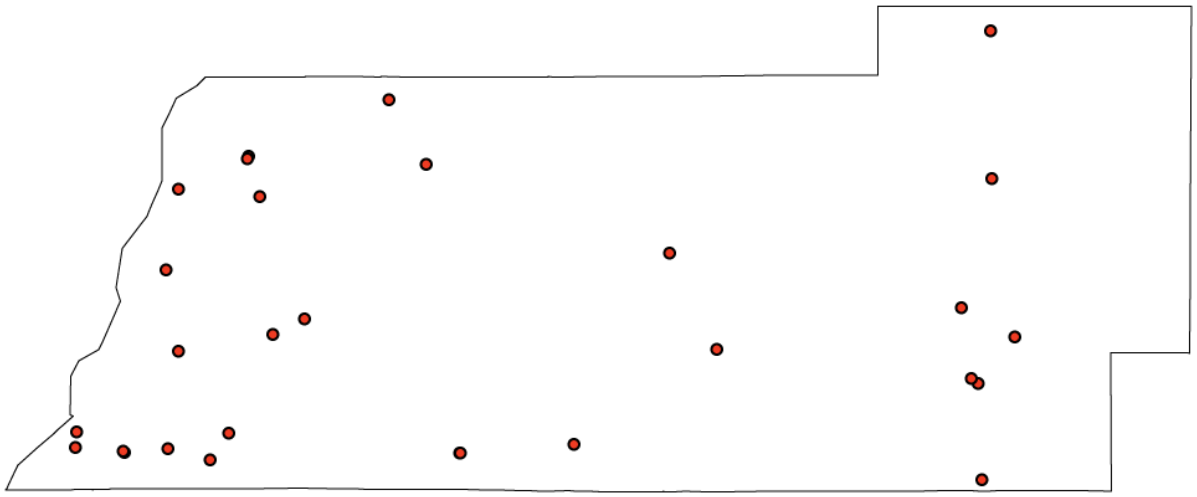

B

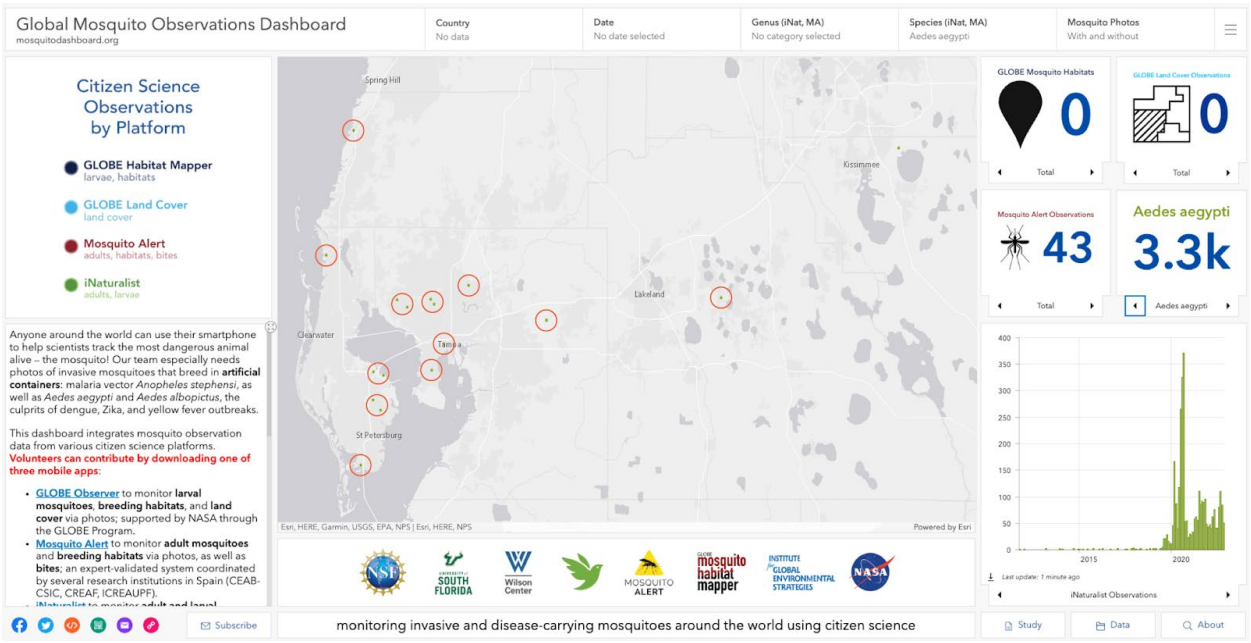

Fig. S1. *Ae. aegypti* data used to validate this study's main models: 856 specimens from 32 trap locations in Pasco County during 2020 (A), and 36 iNaturalist citizen science observations from 16 locations between 2019-2022 (B).

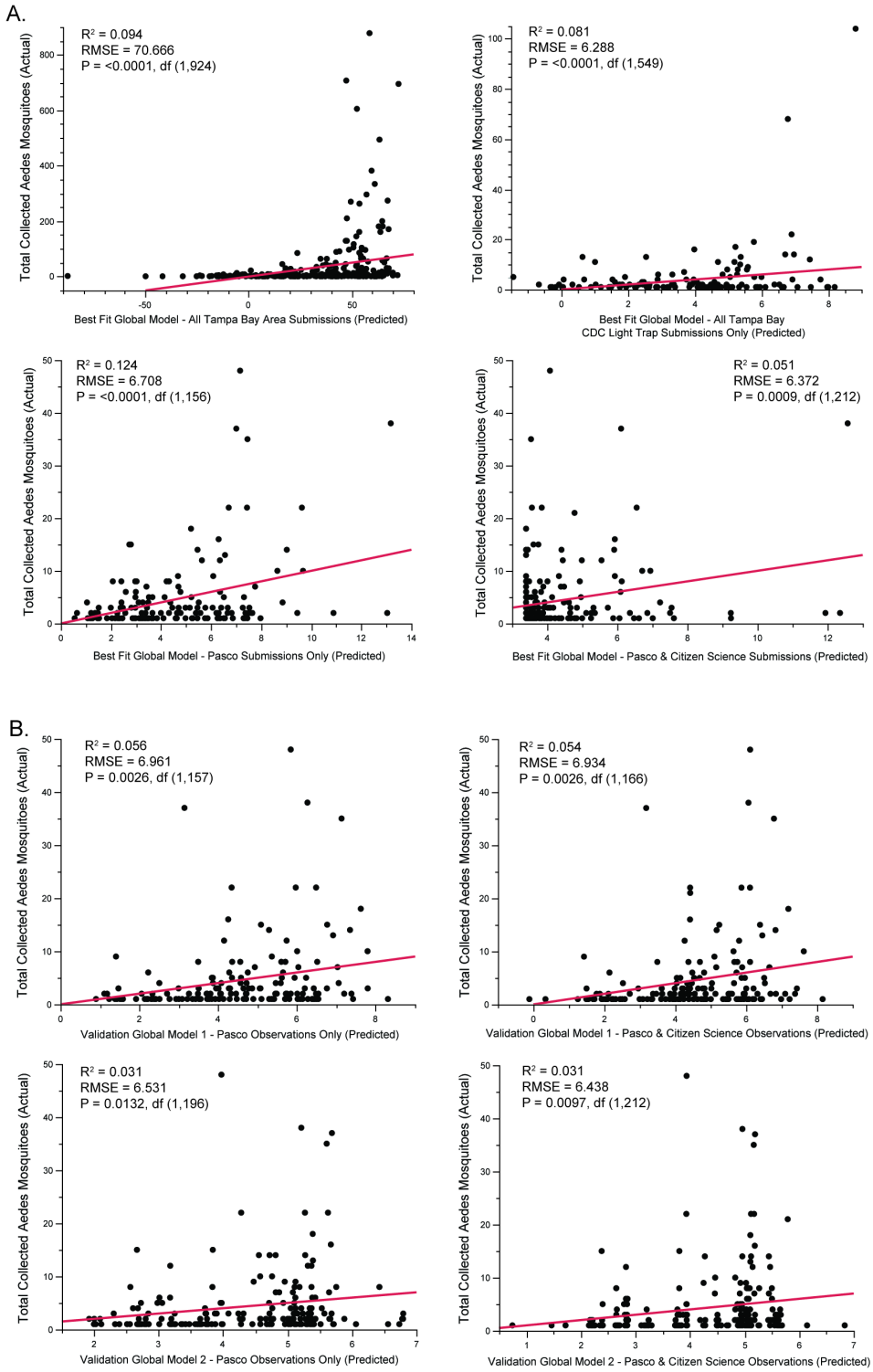

Fig. S2. Global model best fit predicted vs. actual female *Aedes aegypti* mosquitoes collected by type of submissions (A): All Tampa Bay, FL submissions (top left), All Tampa Bay, FL submissions collected by CDC light trap (top right), All 2020 Pasco County collections (bottom left), and all 2020 Pasco County submissions and citizen science observations (bottom right). Global models for all 2017-2019 Tampa Bay, FL area submissions were validated by 2020 Pasco County submissions with and without citizen science observations (B).

SUPPLEMENTARY REFERENCES

Carney, R. M., Mapes, C., Low, R. D., Long, A., Bowser, A., Durieux, D., Rivera, K., Dekramanjian, B., Bartumeus, F., Guerrero, D., Seltzer, C. E., Azam, F., Chellappan, S., & Palmer, J. R. B. (2022). Integrating Global Citizen Science Platforms to Enable Next-Generation Surveillance of Invasive and Vector Mosquitoes. *Insects*, *13*(8). https://doi.org/10.3390/insects13080675

Landsat Missions. (2023). *Landsat Enhanced Vegetation Index*. https://www.usgs.gov/landsat-missions/landsat-enhanced-vegetation-index

Nagler, P. L., Scott, R. L., Westenburg, C., Cleverly, J. R., Glenn, E. P., & Huete, A. R. (2005). Evapotranspiration on western U.S. rivers estimated using the Enhanced Vegetation Index from MODIS and data from eddy covariance and Bowen ratio flux towers. *Remote Sensing of Environment*, *97*(3). https://doi.org/10.1016/j.rse.2005.05.011

National Land Cover Database. (2019). *Multi-Resolution Land Characteristics (MRLC) Consortium*. https://www.mrlc.gov/

Purevdorj, T. S., Tateishi, R., Ishiyama, T., & Honda, Y. (1998). Relationships between percent vegetation cover and vegetation indices. *International Journal of Remote Sensing*, *19*(18). https://doi.org/10.1080/014311698213795

United States Geological Survey Multi-Resolution Land Characteristics Consortium. (2019). *National Land Cover Database 2019*. https://www.mrlc.gov/

U.S. Census Bureau. (2019). *American Community Survey Demographic and Housing Estimates 2014-2019* . https://data.census.gov/table?d=ACS+5-Year+Estimates+Data+Profiles&tid=ACSDP5Y2019.DP05&hidePreview=false

U.S. Census Bureau. (2020a). *American Community Survey Decennial Census: Race*. https://data.census.gov/table?q=P1:+RACE&tid=DECENNIALPL2020.P1&hidePreview=true

U.S. Census Bureau. (2020b). *American Community Survey Median Household Income in the Past 12 Months (In 2020 Inflation-Adjusted Dollars)*. https://data.census.gov/table?q=B19013&g=0400000US12$1400000&tid=ACSDT5Y2020.B19013

U.S. Census Bureau. (2021). *American Community Survey Selected Housing Characteristics*. https://data.census.gov/table?tid=ACSDP1Y2021.DP04